Modeling and control of CO_2 separation process with hollow fiber membrane modules

Hong Gi Jin, Sang Hoon Han, Young Moo Lee, and Yeong Koo Yeo[†]

Department of Chemical Engineering, Hanyang University, Seoul 133-791, Korea
(*Received 25 March 2010 • accepted 3 May 2010*)

Abstract−A multi-stage model is developed for CO_2 separation by hollow-fiber membrane. The model permits rapid solution of the governing differential mass and pressure distribution in hollow-fiber gas separation modules using a computational scheme that does not rely on commercial software and conventional numerical methods such as shooting techniques. For 1-stage, 2-stage and 3-stage configurations the changes of required separation areas according to stage cuts are computed. A simple model predictive control technique is employed to provide optimal operation conditions based on the proposed model. Values of stage cuts can easily be identified for various desired mole fractions and recovery rates. From the results of numerical simulations, we can see that the proposed model can be effectively used in the control of gas separation process by hollow-fiber membrane modules.

Key words: Multi-stage Model, Model Predictive Control, Modeling of Separation Process, Carbon Dioxide, Hollow Fiber Membrane

INTRODUCTION

The use of polymeric membranes for gas separation processes is becoming a standardized unit operation for various applications. One of the most promising applications using membranes is related to separation and recovery of CO_2 from exhaust gas [1]. The cost of CO_2 separation occupies 70-80% of total cost required in CO_2 recovery and storage. Thus, reduction of CO_2 separation cost makes the greatest contribution to improving the economics of the CO_2 treatment industry. Membrane-based CO_2 separation has many advantages over other separation methods: 1) it is energy effective because phase transition is not involved; 2) operation and maintenance are simple because related facilities are compact and small; 3) adjustment of operating conditions and scale-up are relatively easy [2]. Recently, a new membrane with high permeability (about 500 times as high as that of cellulose acetate membrane and about 300 times as high as that of polyimide membrane) was developed to enhance economics of CO_2 separation by membranes [3].

Models are required to evaluate the performance of CO_2 separation by membranes. In this work, we focus on the modeling and control of hollow-fiber membrane modules due to their widespread industrial use for membrane-based gas separation processes. In particular, models for a few configurations of hollow-fiber membrane modules are investigated in this study. Mole fraction of CO_2 in separated gas and recovery rate can be considered as output variables. In this case, the recovery rate is defined as the multiplication of molar flux by mole fraction of CO_2 in feed gas divided by that in exit gas [4].

Noureddlne et al. [5] presented series solutions for co-current and counter-current flow hollow-fiber membrane separation processes [5]. Mathews et al. (1997) proposed models and numerical algorithms for radial cross flow, co-current and counter-current flow

hollow-fiber membrane modules used in gas separation [6]. Results on the design and operation of multiple-stage hollow-fiber membrane separation processes were reported for CO_2 separation with recovery rate of 90% and mole fraction of 99% in the power generation plant using LNG feed [7]. They developed asymmetric hollow-fiber poly-isosulfone membrane modules. Song et al. [8,9] found that the partial pressure of CO_2 in the feed gas, the ratio of pressure between permeating side and membrane, and residence time of feed gas are considered to be the most significant factors affecting permeability performance. They performed numerical analysis on the CO_2 separation characteristics for co-current and counter-current flow hollow-fiber poly-isosulfone membrane modules.

This study presents a multi-stage model that permits rapid solution of the governing differential mass and pressure distributions in a hollow-fiber gas separation modules using a computational scheme that does not rely on commercial software and conventional numerical methods such as shooting techniques. For 1-stage, 2-stage and 3-stage configurations the changes of required separation areas according to stage cuts are computed. Application of a simple model predictive control technique is followed to provide optimal operation conditions based on the proposed model. Values of stage cuts can easily be identified for various desired mole fractions and recovery rates.

EXPERIMENTAL

Hollow fiber has larger membrane area in a unit volume compared with any other type of membrane and is most commonly used in membrane gas separation operations. Commercial hollow fiber membranes can provide less than 0.5 μm of effective thickness, which enables the membrane to show more than 6.7×10^{-10} mol/m²·s·Pa of gas flux from 1 Barrer of membrane permeability. Thus, we can see that a material exhibiting 2000 Barrer of CO_2 permeability can be assumed to have more than 10^{-6} mol/m²·s·Pa of CO_2 flux in a membrane module.

[†]To whom correspondence should be addressed.
E-mail: ykyeo@hanyang.ac.kr

The precursor material of the hollow fiber membrane used in this work is hydroxyl-containing polyimide (HPI) which is prepared by the reaction of 4,4′-hexafluoroisopropylidene diphthalic anhydride (6FDA) and 2,2′-bis(3-amino-4-hydroxyphenyl) hexafluoropropane (bisAPAF) [3]. This HPI can be thermally converted into polybenzoxazole (PBO) by chain rearrangement, where the polymer chains can give rise to high free volume elements corresponding with high gas permeability.

Using dry-wet phase inversion method, hollow fiber membranes were prepared by extruding a dope solution composed of precursor polymer, N-methylpyrrolidinone (NMP) as a solvent and tetrahydrofuran (THF) as a volatile non-solvent. Fig. 1 shows a typical hollow fiber spinning instrument. After the dope solution was spun from a spinneret connected to a gear pump as shown in Fig. 1, the hollow fiber membranes were wound to a cylindrical bobbin in an overflowing warm water bath until the residual solvents were fully eliminated by solvent exchange. The hollow fiber membrane was dried overnight at 150 °C, thermally rearranged in a muffled furnace at 450 °C and one hour, put in a membrane module made up of sustainable stainless steel (SUS), and finally sealed with epoxy adhesives.

Fig. 1. Schematic diagram of hollow fiber spinning instrument.

Fig. 2 shows a schematic diagram for the membrane permeation test. Performance of the hollow fiber membrane module was measured in a temperature-controlled apparatus which can regulate the pressure and flow rate of each stream. For four streams (upstream in-let, upstream retentate, downstream sweep and downstream permeate), Kofloc 3660 and 3760 for mass flow controllers (MFCs) and meters (MFMs) (Kojima Instruments Inc., Kyoto, Japan) and Baratron 626A (1,000 torr) and 722A (20,000 torr) (MKS Instrument Corp., MA, USA) for pressure measurement were connected to a pressure and flow controller, MR-5000 (MJ Technics Co. Ltd., Incheon, Korea). The data were acquired continuously via RS-232 cable by Labview 7.1 software (National Instrument Corp., Austin, TX, USA). Each component was assembled with 1/4 inch SUS 316 tubes, tube fittings, 2-way and 3-way valves as shown in Fig. 2.
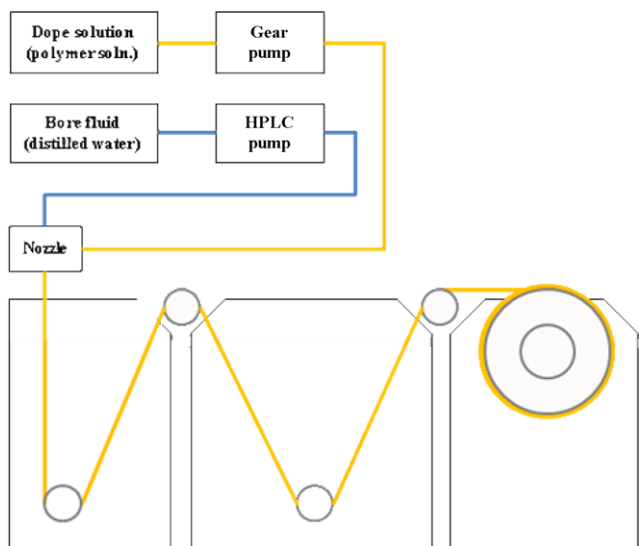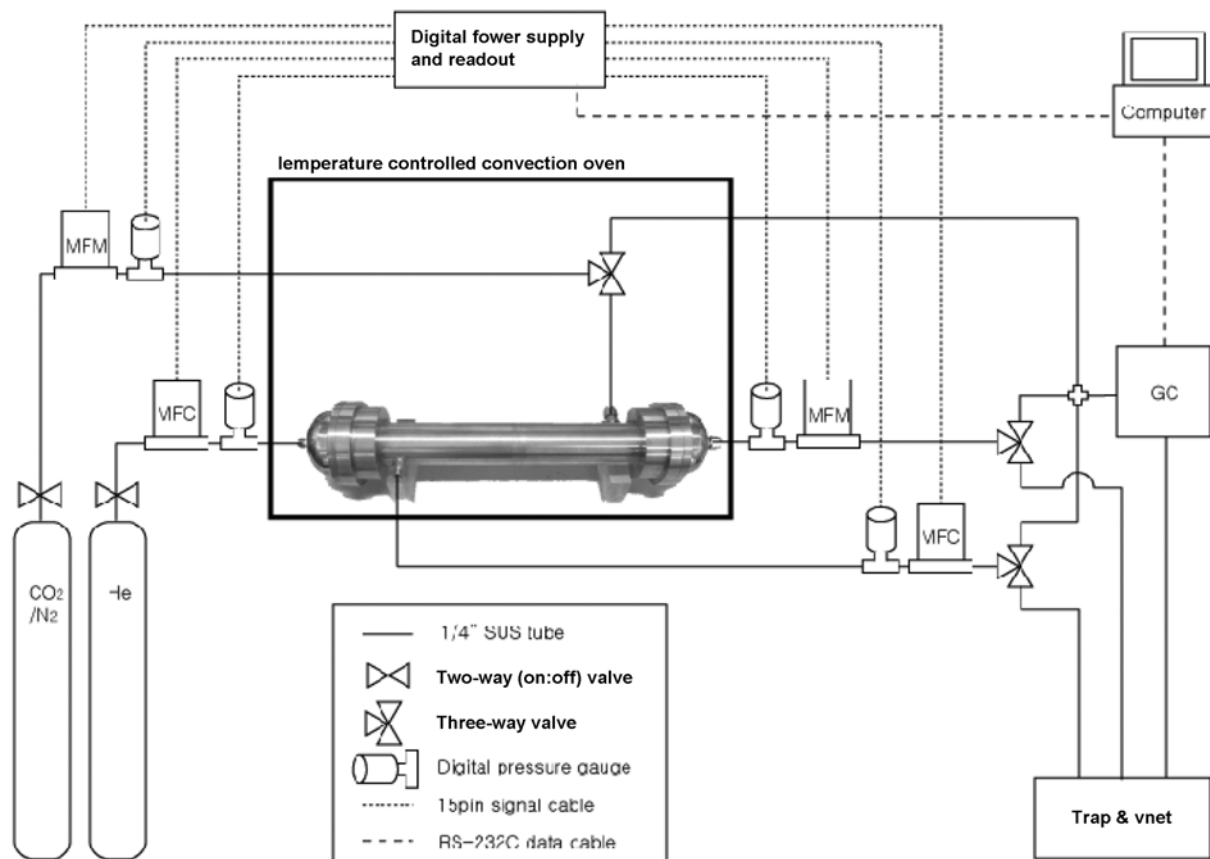

Fig. 2. Schematic diagram for membrane permeation test.

A gas chromatograph (GC-2010ATF, Shimadzu Corp., Kyoto, Japan) with an electrically controlled six-channel loop (Vici Valco Instruments Co. Inc., Houston, TX, USA) was introduced to analyze the composition of each stream. The loop was opened in 30 sec and filled with the gas mixtures, then closed and swept into detector by helium. Mixed gases with different compositions in in-let, retentate and permeate stream were separated in a Porapak Q packed column and detected in thermal conductive detector (TCD) detector every 3 minutes.

A gas mixture composed of 15 mol% of carbon dioxide and balanced nitrogen was used as a simulated flue gas at upstream in-let stream, and high purity of helium (99.99+%) was used for sweep gas at downstream. In-let gas pressure was varied from 1 to 7 atm to make difference in the pressure ratio and then optimized. At the retentate stream, gas flow rate was controlled to calculate the exact stage-cut, and pressure was measured to quantify a possible pressure drop compared to the in-let pressure. At the permeate stream, MFM rather than MFC was used so that the flow was not disturbed by the measurement instrument.

MATHEMATICAL MODEL

Fig. 3 shows the flow configuration ((a) counter-current flow, (b) co-current flow) and external structure of a typical hollow-fiber gas separation module. The hollow-fiber bundle is sealed on both ends and is contained inside a high-pressure housing. Feed gas may be introduced on the bore of the hollow-fibers or on the shell side of the module. In the counter-current flow module, helium gas may be introduced in the opposite direction with feed gas. The helium gas may be introduced parallel to the feed gas in the co-current flow module. For counter-current flow module, the difference in the driv-

ing force between the inlet and the outlet is negligible, while for co-current flow module the driving force decreases gradually from the inlet to the outlet [10]. For this reason, the counter-current flow module in general exhibits better separation performance as well as better operational flexibility, and only the counter-current flow module is considered in this study. The principal assumptions underpinning the model are:

◆ Shell side pressure change is negligible.

◆ The hollow-fibers consist of a very thin membrane separation layer. All mass transfer resistance is confined to the separation membrane or the total membrane wall.

◆ There is no axial mixing of shell in the direction of bulk gas flow.

◆ The gas on the shell side of the hollow-fibers is in plug flow.

◆ The deformation of the hollow-fiber under pressure is negligible.

◆ All fibers have uniform inner and outer radius as well as a uniform thickness separation membrane.

◆ The membrane module is operated at steady-state.

1. Single-stage Module

Fig. 4 shows a single membrane module with complete mixing. When a separator element is operated at a low recovery, there is a minimal change in composition. In this case the results derived using the complete-mixing model provide reasonable estimates of permeate purity. The overall material balance can be written as:

$$q_f = q_o + q_p \tag{1}$$

The stage-cut θ, the fraction of feed permeated, is defined as:
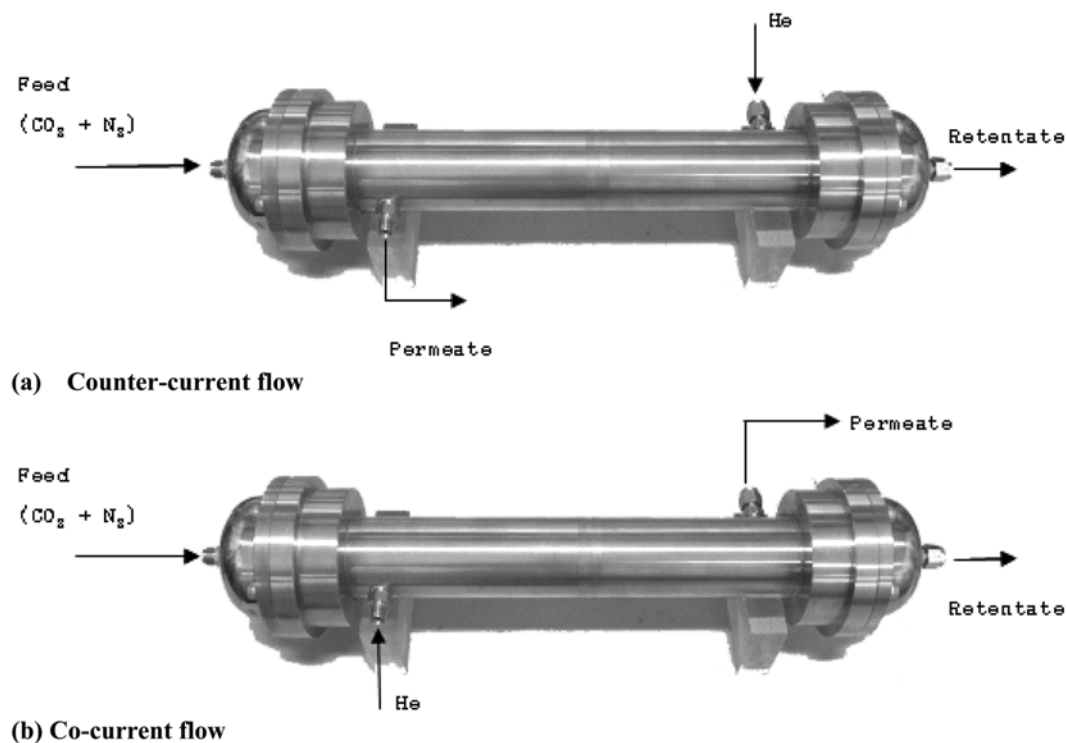
$$\theta = \frac{q_p}{q_f} \tag{2}$$

Fig. 3. Configuration of hollow-fiber membrane module: (a) Counter-current flow, (b) Co-current flow.
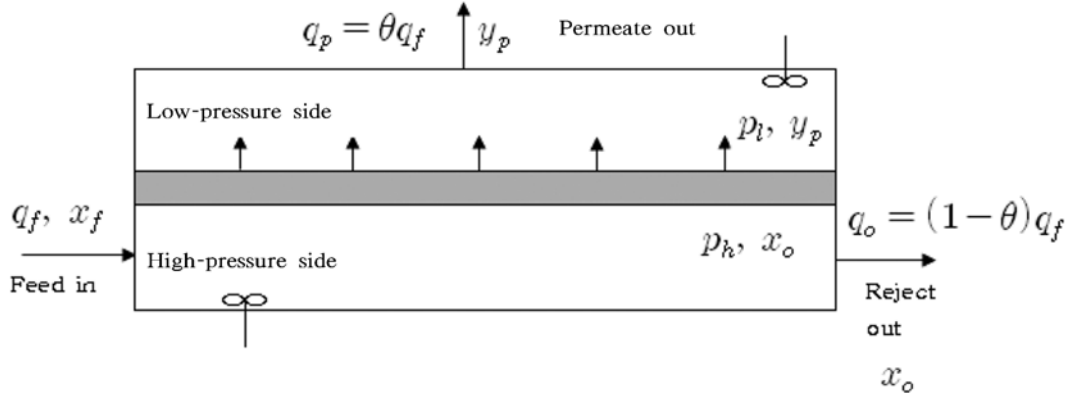
H. G. Jin et al.

Fig. 4. Membrane separation with complete mixing.

The rate of diffusion or permeation of CO_2 is given by:

$$\frac{q_{CO_2}}{A_m} = \frac{q_p y_p}{A_m} = \left(\frac{P_{CO_2'}}{t}\right)(p_h x_o - p_l y_p) \tag{3}$$

Similar equations can be used for N_2 permeation.

$$\frac{q_{N_2}}{A_m} = \frac{q_p(1-y_p)}{A_m} = \left(\frac{P_{N_2'}}{t}\right)[p_h(1-x_o) - p_l(1-y_p)] \tag{4}$$

Dividing Eq. (3) by Eq. (4) gives

$$\frac{y_p}{(1-y_p)} = \frac{\alpha^*[x_o - (p_l/p_h)y_p]}{(1-x_o)-(p_l/p_h)(1-y_p)} \tag{5}$$

This equation relates the permeate concentration y_p to the reject concentration x_o. The ideal separation factor α^* is defined by:

$$\alpha^* \equiv \frac{p_{CO_2'}}{p_{N_2'}} \tag{6}$$

Making the overall material balance for CO_2, we have

$$q_f x_f = q_o x_o + q_p y_p \tag{7}$$

Dividing by q_f and solving for exit reject gas composition, we have

$$x_o = \frac{x_f - \theta y_p}{(1-\theta)} \quad \text{or} \quad y_p = \frac{x_f - x_o(1-\theta)}{\theta} \tag{8}$$

Substituting $q_p = \theta q_f$ (from Eq. (2)) into Eq. (3) and solving for the membrane area, A_m, we get

$$A_m = \frac{\theta q_f y_p}{\left(\frac{p_{CO_2'}}{t}\right)(p_h x_o - p_l y_p)} \tag{9}$$

If x_f, θ, α^*, and p_l/p_h are given and y_p, x_o, and A_m are to be determined, we solve for y_p using the quadratic equation to give

$$y_p = \frac{-b_1 + \sqrt{b_1^2 - 4a_1c_1}}{2a_1} \tag{10}$$

where

$$a_1 = \theta + \frac{p_l}{p_h} - \frac{p_l}{p_h}\theta - \alpha^*\theta - \alpha^*\frac{p_l}{p_h} + \alpha^*\frac{p_l}{p_h}\theta$$

$$b_1 = 1 - \theta - x_f - \frac{p_l}{p_h} + \frac{p_l}{p_h}\theta + \alpha^*\theta + \alpha^*\frac{p_l}{p_h} - \alpha^*\frac{p_l}{p_h}\theta + \alpha^* x_f$$
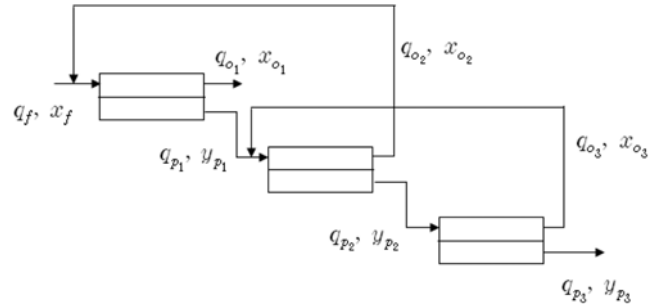
Fig. 5. Three-stage membrane separation system.

After solving for y_p, the value of x_o is calculated from Eq. (8) and A_m from Eq. (9). The recovery ratio is defined by:

$$\text{recovery} = \frac{q_p y_p}{q_f x_f} \tag{11}$$

2. Multi-stage Module

Modeling of a multi-stage separation system requires additional material balances in addition to the material balance for each stage. Fig. 5 shows a three-stage configuration of a membrane separation module with recycle to the prior stage at each stage. The permeate gas from the previous stage becomes the feed gas to the next stage and the reject gas after 2nd-stage is recycled to the previous stage to be the feed gas.

For a two-stage system, the total feed flow rate and the mole fraction of CO_2 to the 1st-stage are given by:

$$q_{f_1} = q_f + q_{o_2} \tag{12}$$

$$x_{f_1} = \frac{q_f x_f + q_{o_2} x_{o_2}}{q_f + q_{o_2}} \tag{13}$$

The total feed flow rate and the mole fraction of CO_2 to the 2nd-stage are given by:

$$q_{f_2} = q_{p_1} \tag{14}$$

$$x_{f_2} = y_{p_1} \tag{15}$$

For a three-stage system, the total feed flow rate and the mole fraction of CO_2 to the 1st-stage are given by:

$$q_{f_1} = q_f + q_{o_2} \tag{16}$$

$$x_{f_1} = \frac{q_f x_f + q_{o_2} x_{o_2}}{q_f + q_{o_2}} \tag{17}$$

The total feed flow rate and the mole fraction of CO_2 to the 2nd-stage are given by:

$$q_{f_2} = q_{p_1} + q_{o_3} \tag{18}$$

$$x_{f_1} = \frac{q_{p_1} y_{p_1} + q_{o_3} x_{o_3}}{q_{p_1} + q_{o_3}} \tag{19}$$

The total feed flow rate and the mole fraction of CO_2 to the 3rd-stage are given by:

$$q_{f_3} = q_{p_2} \tag{20}$$

$$x_{f_3} = y_{p_2} \tag{21}$$

3. Transfer Function Model for Model Predictive Control

To get transfer function models, we start with derivation of dimensionless governing equations. We first define some dimensionless variables:

$$L^* \equiv \frac{L}{L_f} \tag{22}$$

$$V^* \equiv \frac{V}{L_f} \tag{23}$$

$$A_m \equiv \pi D_{LM} l = \pi D_{LM} l^* l_m \tag{24}$$

$$\gamma_1 \equiv \frac{p_h}{p_f} = \frac{p_l}{\gamma p_f} \tag{25}$$

$$\gamma_2 \equiv \frac{p_l}{p_f} = \frac{\gamma p_h}{p_f} \tag{26}$$

$$K_1 \equiv \pi D_{LM} \frac{l_m}{L_f} \left(\frac{p_B'}{t} \right) p_f \tag{27}$$

$$K_2 \equiv \frac{128 \mu R T L_f l_m}{\pi p_f^2 d_i^4} \tag{28}$$

Using the dimensionless variables defined above, we can get dimensionless governing equations:

$$\frac{dL^*}{dt} = -K_1 [\alpha^* (\gamma_1 x - \gamma_2 y) + \gamma_1 (1-x) - \gamma_2 (1-y)] \left(\frac{L_f L^*}{l_m \pi d_i^2} \right) \tag{29}$$

$$\frac{dV^*}{dt} = K_1 [\alpha^* (\gamma_1 x - \gamma_2 y) + \gamma_1 (1-x) - \gamma_2 (1-y)] \left(\frac{L_f L^*}{l_m \pi d_i^2} \right) \tag{30}$$

$$\frac{dx}{dt} = -\frac{K_1}{L^*} [\alpha^* (\gamma_1 x - \gamma_2 y) - x [\alpha^* (\gamma_1 x - \gamma_2 y) + \gamma_1 (1-x) - \gamma_2 (1-y)]] \left(\frac{L_f L^*}{l_m \pi d_i^2} \right) \tag{31}$$

$$\frac{dy}{dt} = \frac{K_1}{V^*} [\alpha^* (\gamma_1 x - \gamma_2 y) - y [\alpha^* (\gamma_1 x - \gamma_2 y) + \gamma_1 (1-x) - \gamma_2 (1-y)]] \left(\frac{L_f L^*}{l_m \pi d_i^2} \right) \tag{32}$$

$$\frac{d\gamma_1}{dt} = -K_2 \frac{L^*}{\gamma_1} \left(\frac{L_f L^*}{l_m \pi d_i^2} \right) \tag{33}$$

Based on dimensionless governing equations, the transfer func-

tion model representing effects of stage-cuts on the recovery rate can be given by 2nd-order with time delay model:

$$G_1 = \frac{3.641}{1227s^2 + 127.5s + 1} e^{-1.01s} \tag{34}$$

Therefore we have

$$y_1 = G_1 u \tag{35}$$

Similarly, the transfer function model representing effects of stage-cuts on the mole fraction can be given by 1st-order with time delay model:

$$G_2 = \frac{2.713}{225.6s + 1} e^{-62.5s} \tag{36}$$

Therefore we have

$$y_2 = G_2 u \tag{37}$$

RESULTS AND DISCUSSIONS

1. Simulation of Single-stage System

Table 1 shows the parameters and data used in the numerical simulations. Fig. 6 shows results of numerical simulations as well as those of experiments. We can see that the proposed models exhibit good

Table 1. Parameters used in numerical simulations

Type	Value
p_f	1.4 [bar]=140000 [Pa]
p_l	0.2 [bar]=20000 [Pa]
α^*	25 [-]
x_f	0.15 [-]
q_f	500 [m³/hr]=80357142.86 [mol/hr]
T	25 [°C]=298.15 [K]
R	8.314 [J/mol·K]
(p_{CO_2}'/t)	10^{-6} [mol/m²·s·Pa]=3.6×10^{-3} [mol/m²·hr·Pa]
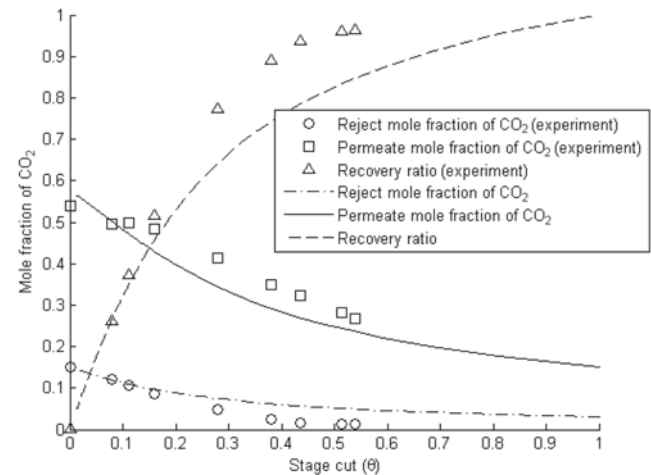
Fig. 6. Recovery and mole fraction of CO_2 at permeate and retentate side in terms of stage cut: x_f=0.15, T=298.15 K, A=1.813 m², P_f=500 kPa, γ_2=0.2.

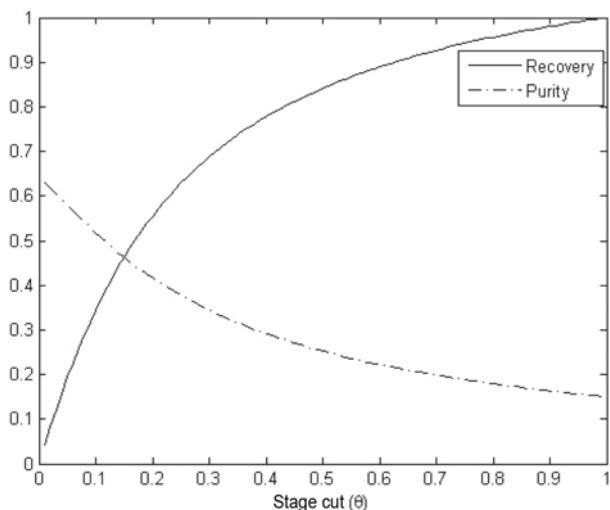Fig. 7. Behavior of recovery and purity with respect to stage-cut in single-stage system.

Fig. 9. Behavior of recovery and purity with respect to stage-cut in two-stage system.

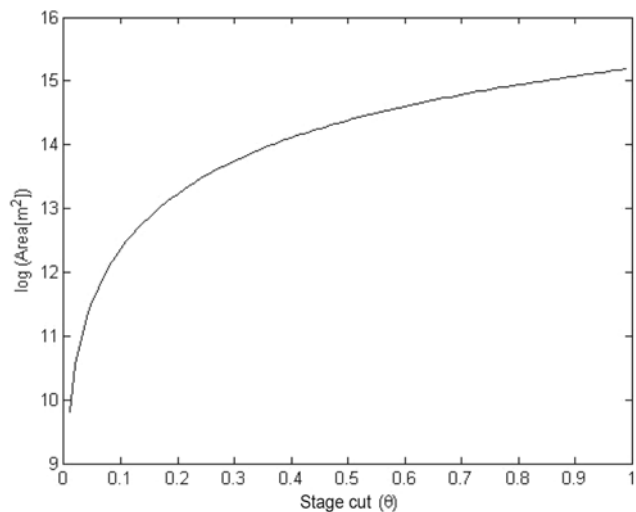

Fig. 8. Required membrane area in single-stage system.

Fig. 10. Required membrane area in two-stage system.

tracking performance to experimental results, which validates the use of the proposed models for hollow-fiber membrane gas separation processes. Here purity means the CO_2 concentration of the permeated stream. Fig. 7 shows changes of CO_2 recovery rate and purity as functions of stage-cut in the range of 0.01-0.99. The recovery rate increases from 0.0421 to 0.9982, while the purity decreases from 0.6313 to 0.1512. The "compromise" point is reached when the stage-cut is 0.15 in which both the recovery rate and purity are 0.4631. Fig. 8 shows the required membrane areas represented in log scale. The area for the stage-cut of 0.15 is 387430 m^2.

2. Simulation of Multi-stage System

For the two-stage module, the stage-cut of the 1st-stage was fixed to 0.26 and changes of the recovery rate and the purity were examined according to the stage-cut. Fig. 9 shows changes of recovery rate and purity as functions of stage-cut of the 2nd-stage in the range of 0.01-0.99 for the two-stage module. The recovery rate increases from 0.0191 to 0.5687, while the purity decreases from 0.8753 to 0.3306. The compromise point is reached when the stage-cut of the
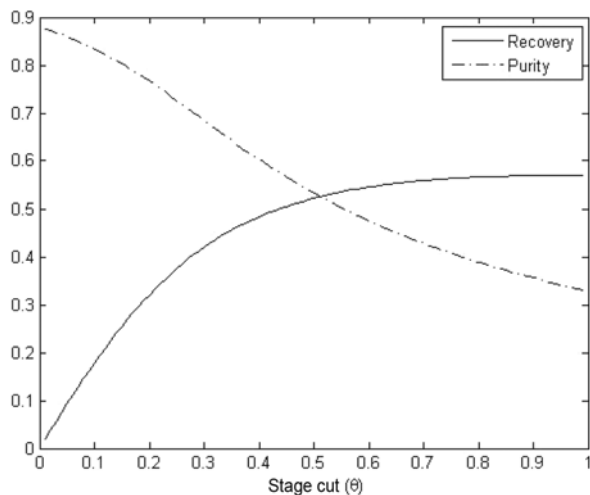

Fig. 11. Behavior of recovery and purity with respect to stage-cut in three-stage system.
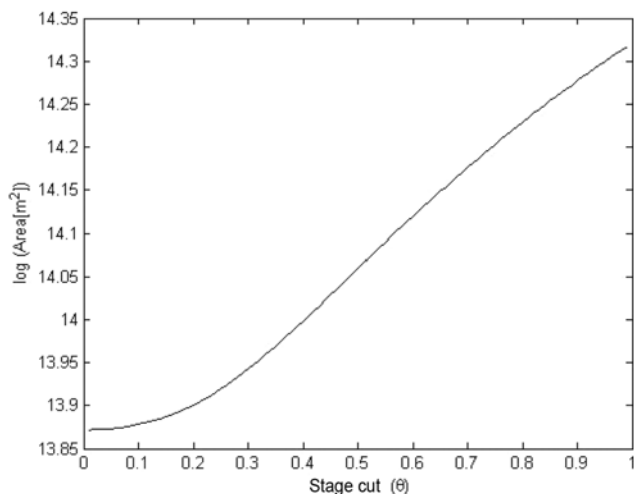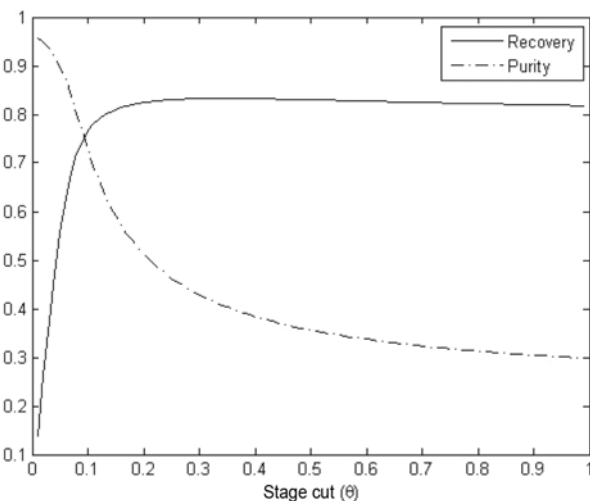
2nd-stage is 0.51 in which both the recovery rate and purity are 0.52. Fig. 10 shows the total required membrane areas represented in log scale. The area for the stage-cut of 0.51 is 1283900 m^2.

For the three-stage module, the stage-cut of the 1st-stage was fixed to 0.50 and that of the 2nd-stage was fixed to 0.70. Again, we examined changes of the recovery rate and the purity according to the stage-cut of the third-stage. In this case the purity means the CO$_2$ concentration of the permeated stream from the third-stage. Fig. 11 shows changes of CO$_2$ recovery rate and purity as functions of stage-cut of the third-stage in the range of 0.01-0.99 for the three-stage module. The recovery rate exhibits initial increase followed by decrease and shows maximal recovery rate of 0.8327. The purity decreases from 0.9576 to 0.2984. The compromise point is reached when the stage-cut of the third-stage is 0.09 in which both the recovery rate and purity are 0.75. Fig. 12 shows the total required membrane areas represented in log scale. The area for the stage-cut of 0.09 is 9185400 m^2.
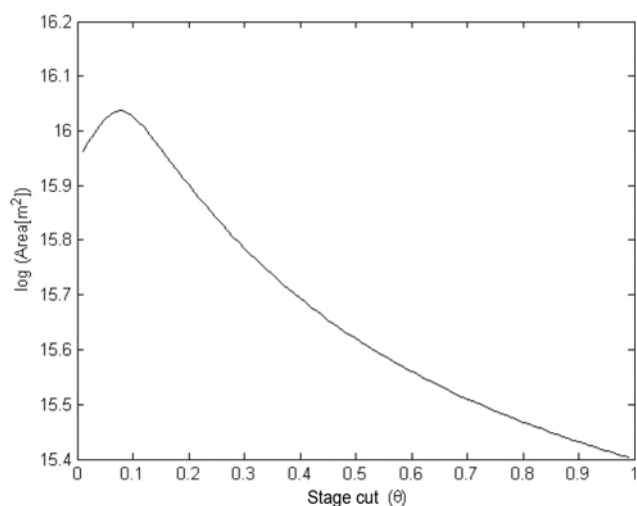

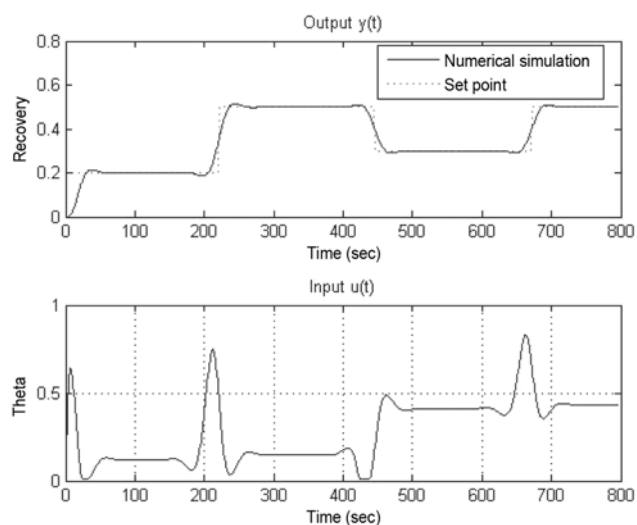Fig. 12. Required membrane area in three-stage system.

Fig. 13. Results of model predictive control for set point changes in recovery.
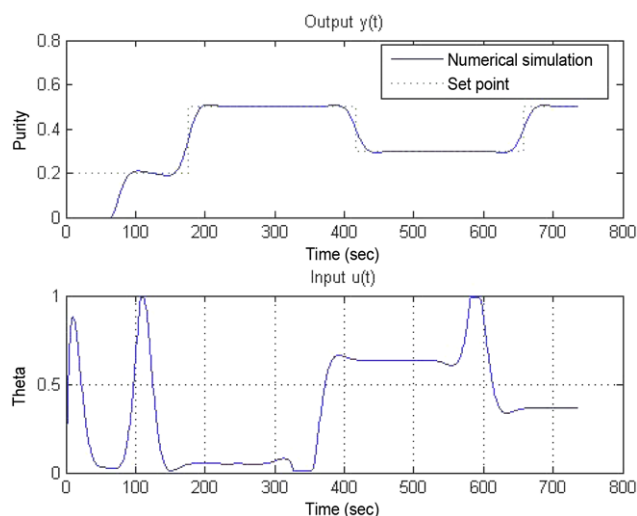

Fig. 14. Results of model predictive control for set point changes in purity.

Table 2. MPC parameters used in this work

Type	Value
Sampling time	1
Prediction horizon	100
Control horizon	2
MV1(input) constraints	0.01-0.99
MO1(output) constraints	0-1

3. Model Predictive Control

A simple model predictive control scheme was employed for various set point changes in recovery rate and purity. Values of stage-cut (θ) were computed as optimal manipulated variables. Fig. 13 shows results of simulations when step changes are introduced into the recovery rate set point. Because of the relative short time delay, input variables (stage-cut) show sharp peaks. Fig. 14 shows results of simulations when step changes are introduced into the purity set point. We can see that satisfactory tracking performance is achieved, which demonstrates that the proposed model can be effectively used in the control of the gas separation process by hollow-fiber membrane modules.

CONCLUSION

We developed a multi-stage model that permits rapid solution of the governing differential mass and pressure distribution in hollow-fiber gas separation modules based on experimental data. We employed a computational scheme that does not rely on commercial software and conventional numerical methods such as shooting techniques. For 1-stage, 2-stage and 3-stage configurations the changes of required separation areas according to stage cuts are computed. A simple model predictive control technique is used to provide optimal operation conditions based on the proposed model. Values of stage cuts can easily be identified for various desired mole fractions and recovery rates. From the results of numerical simulations, we can see that the proposed model can be effectively used in the

control of gas separation by hollow-fiber membrane modules.

NOMENCLATURE

A_m : effective membrane area [m^2]
d_i : inside diameter of hollow fibers [μm]
K_1 : constants defined in Eq. (27) [-]
K_2 : constants defined in Eq. (28) [-]
l_m : total length of hollow fiber [m]
L_f : fresh feed molar flow rate to the permeator [mol/s]
L^* : dimensionless local feed molar rate, Eq. (22) [-]
q_f : flow rate of the feed side [mol/hr]
q_o : flow rate of the reject side [mol/hr]
q_p : flow rate of the permeate side [mol/hr]
p_h : higher pressure [Pa]
p_l : lower pressure [Pa]
R : gas constants [J/mol·K]
(P_{CO_2}'/t) : specific permeability of species CO_2 through hollow fibers [mol/m^2·hr·Pa]
(P_{N_2}'/t) : specific permeability of species N_2 through hollow fibers [mol/m^2·hr·Pa]
T : absolute temperature [K]
t : time [s]
V^* : dimensionless local permeate molar flow rate, Eq. (23) [-]
x : local mole fraction of the more permeable component on the feed side [-]
x_f : mole fraction of CO_2 at the feed side [-]
x_o : mole fraction of CO_2 at the reject side [-]
y : local mole fraction of the more permeable component on the permeate side [-]
y_p : mole fraction of CO_2 at the permeate side [-]
α^* : ideal selectivity defined in Eq. (6) [-]
γ_1 : pressure ratio defined in Eq. (25) [-]
γ_2 : pressure ratio defined in Eq. (26) [-]
π : the ratio of the circumference of a circle to its diameter [-]
θ : stage-cut defined in Eq. (2) [-]

REFERENCES

1. E. S. Kim, D. U. Park and Y. I. Jeong, *CO₂ reduction business*, KISTI (2003).
2. S. Freni, S. Cavallaro, S. Donato, V. Chiodo and A. Vita, *Mater. Lett.*, **58**, 1865 (2004).
3. H. B. Park, C. H. Jung, Y. M. Lee, A. J. Hill, S. J. Pas, S. T. Mudie, E. V. Wagner, B. D. Freeman and D. J. Cookson, *Science*, **318**, 254 (2007).
4. Z. Li, R. Ernst, M. Reinhard, B. Ludger and S. Detlef, *J. Membr. Sci.*, **325**, 284 (2008).
5. B. Noureddlne, S. Amltava and S. Kamalesh, *Ind. Eng. Chem. Fundam.*, **25**, 217 (1986).
6. M. J. Thundyil and W. J. Koros, *J. Membr. Sci.*, **125**, 275 (1997).
7. S. H. Choi, J. H. Kim, B. S. Kim and S. B. Lee, *Membrane J.*, **15**(4), 310 (2005).
8. I. H. Song, H. S. Ahn, Y. J. Lee, H. S. Jeon, Y. T. Lee, J. H. Kim and S. B. Lee, *Membrane J.*, **16**(3), 204 (2006).
9. I. H. Song, H. S. Ahn, Y. J. Lee, H. S. Jeon, Y. T. Lee, J. H. Kim and S. B. Lee, *Membrane J.*, **16**(4), 252 (2006).
10. R. D. Noble and S. A. Stern, *Membrane separations technology - principles and applications*, Elsevier Science B.V., 519-528 (1995).